Microchimica Acta (2022) 189: 297
https://doi.org/10.1007/s00604-022-05387-2

ORIGINAL PAPER

Hemin-graphene oxide-gold nanoflower-assisted enhanced electrochemiluminescence immunosensor for determination of prostate-specific antigen

Gengjun Liu[1] · Xiaohan Guan[2] · Binxiao Li[3] · Hong Zhou[1,4] · Na Kong[5] · Haiyan Wang[1]

Received: 13 April 2022 / Accepted: 19 June 2022 / Published online: 28 July 2022

Abstract

An ultrasensitive luminol electrochemiluminescence (ECL) immunosensor was constructed for the detection of prostate specific antigen (PSA) using glucose oxidase–decorated hemin-graphene oxide-gold nanoflowers ternary nanocomposites as probes. Graphene oxide was first modified with hemin and then with gold nanoflowers through an in situ growth method, which has significantly boosted the catalytic activity of this graphene oxide–based peroxidase mimetics. The biocatalytical activity of this ECL immunosensor was thoroughly investigated to achieve selective recognition of the analyte molecules (PSA) by specific binding between antigens and antibodies. The limit of detection was calculated to be 0.32 pg mL^{-1} with a signal-to-noise ratio of 3. A broad linear range from 7.5×10^{-4} to 2.5 ng mL^{-1} was obtained. Such step-by-step assembled biosensor showed controlled nanostructure and exhibited promising application in analysis of human serum samples with a recovery range of 90.6–111.8% and a RSD range of 3.9–5.5%.

Keywords Electrochemiluminescence (ECL) biosensor · Hemin-graphene oxide-gold nanoflowers · Prostate-specific antigen · Peroxidase mimetics · Luminol

Introduction

Sensitive and accurate detection of biomarkers shows an increasing importance in early diagnosis of diseases, biomedical analysis, and biodefense research [1–4]. Numerous techniques such as electrochemiluminescent (ECL) biosensor, fluorescent labeling, enzyme-linked immunosorbent assay surface, and plasmon resonance have been reported due to their rapid identification and sensitive quantitation among broad biological molecules [5–8]. Among these methods, ECL immunoassay has gained great attention due to its advantages of low background, easy operation, good controllability, and high detection sensitivity [9]. In the ECL immunoassay system, ECL luminophores mainly include inorganic ruthenium and iridium complexes, organic luminol, and nanomaterials. For example, many types of nanomaterials have been selected as the signal probe in the ECL immunoassay, such as lanthanide (Ln) metal–organic frameworks with the admirable self-luminescence properties

Gengjun Liu and Xiaohan Guan contributed equally to this work.

✉ Hong Zhou
zhouhong@qust.edu.cn

✉ Na Kong
kongna109101@126.com

✉ Haiyan Wang
why_phd@163.com

[1] Department of Blood Transfusion, The Affiliated Hospital of Qingdao University, Qingdao 266042, People's Republic of China

[2] Clinical Medicine Department, Medical College, Qingdao University, Qingdao 266071, People's Republic of China

[3] Department of Chemistry, Shanghai Stomatological Hospital, State Key Laboratory of Molecular, Engineering of Polymers and Institute of Biomedical Sciences, Fudan University, Shanghai 200433, People's Republic of China

[4] Key Laboratory of Optic-Electric Sensing and Analytical Chemistry for Life Science, Ministry of Education, College of Chemistry and Molecular Engineering, Qingdao University of Science and Technology, Qingdao 266042, People's Republic of China

[5] Agricultural Products Processing Research Institute, Chinese Academy of Tropical Agricultural Sciences, Zhanjiang 524001, People's Republic of China

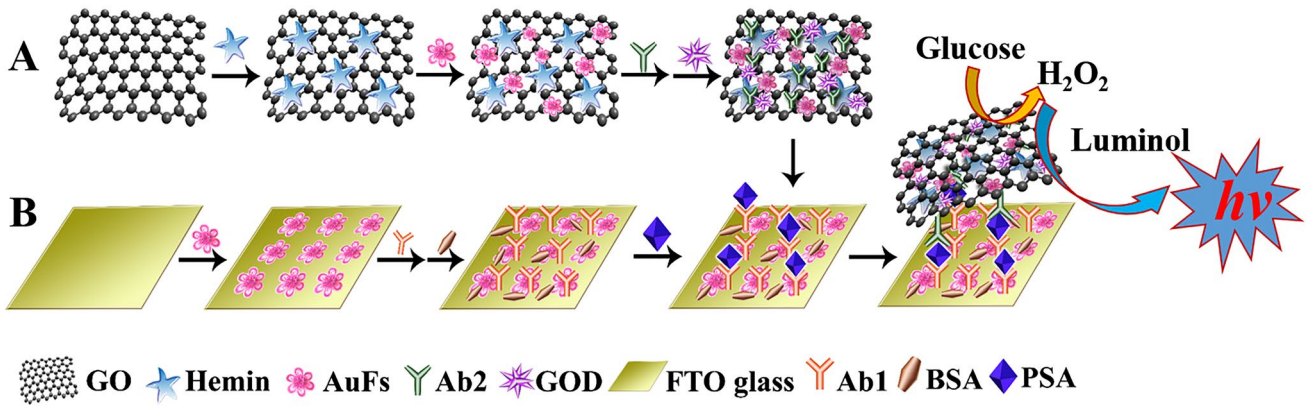

Scheme 1 The PSA biosensing platform based on H-RGO-AuF composites. Processes A and B respectively represent the preparation of hemin-reduced graphene oxide-Au nanoflowers (H-RGO-AuFs) and PSA biosensing platform

[10]. Recently, some strategies, for example target assistant proximity hybridization strategy [11], $Ru(bpy)_3^{2+}$-loaded mesoporous silica nanoparticles [12], or luminol-loaded graphitic carbon nitride nanosheets [13], have been reported to enhance the performance of ECL immunoassay in specificity and sensitivity. Luminol-based ECL systems show very broad applications due to its low excitation potential, high quantum yield, and nontoxicity. However, natural glucose oxidase (GOD) catalyze glucose is generally used to generate H_2O_2 working as co-reactant of luminol-based ECL systems, which leads to many problems including poor electron transfer behavior and unsatisfied stability which greatly limited its application.

To overcome these problems, hybrid nanomaterial-based peroxidase mimetics attracted much attention by combining of biological molecules with nanomaterial components such as metal nanoparticles [14–16], graphene family nanomaterials [17–19], quantum dots [20–22], and other novel nanomaterials [10, 23, 24]. Nanomaterials could not only retain the bioactivity of immobilized biomolecules due to the desirable microenvironments but also serve as electrical bridges that communicate with the biomolecules and the working electrodes [25, 26]. For example, graphene oxide (GO) with large surface area, high electric conductivity, and excellent biological compatibility exhibits promising application in synthesizing hybrid peroxidase mimetics in the construction of microelectronic biosensors [26–29]. With further combination of metal nanoparticles including gold nanoparticles, Pt–Pd bimetallic nanoparticles, and Fe_3O_4 magnetic nanoparticles, enhanced catalytic activity and stability could be obtained [30–33].

Our recent work synthesized a composite by in situ formation of Au nanoflowers (AuFs) on the surface of hemin functionalized GO (H-RGO) [34] and found this composite with nanosucculent morphology of AuFs performed higher catalytic ability with enhanced kinetic parameter than that of composite with traditional Au nanoparticles with smooth surface on graphene [35]. The superior features of AuFs exhibit great potential application in biomolecule detection. Herein, in this work, we applied this high electrocatalytic ternary composite hemin-reduced graphene oxide-Au nanoflowers (H-RGO-AuFs) and constructed a detecting method for prostate specific antigen (PSA) through a coreactant ECL immunoassay strategy (Scheme 1). In order to achieve robust ECL enhancement, AuFs were employed as probes and working substrate. The synthesized Ab_2-probes were bonded with the PSA terminated FTO-AuF substrate by the specific recognition and formed a sandwich-type conjugation. The stepwise fabrication of ECL sensor and enzymatic activities of final probes were systematically investigated through electron microscopy, UV–vis, and electrochemistry measurements. The results showed that this sensing platform was sensitive with PSA exclusively.

Experimental section

Reagents and materials

Graphene oxide (GO) dispersion was purchased from Nanjing XFNANO Materials Tech Co., Ltd. From Sigma-Aldrich Inc. (USA), we ordered the luminol, hematin, and $HAuCl_4{\cdot}4H_2O$. GOD, human PSA, and mouse antihuman total PSA monoclonal antibodies (primary capture antibody, Ab_1, and secondary detection antibody, Ab_2) were purchased from Linc-Bio Science Co., Ltd. (Shanghai). Carcinoembryonic antigen (CEA), alpha-fetoprotein (AFP), bovine serum albumin (BSA), N-hydroxysuccinimide (NHS), and N-(3-dimethylaminopropyl)-N′-ethyl-carbodiimide hydrochloride (EDC) were purchased from Aladdin-Reagent Co., Ltd. (Shanghai, China). Fluorine-doped tin oxide (FTO)–coated glass (1.1 mm thickness, 100 × resistances) was obtained

from Kaivo (Zhuhai, China). 0.01 M phosphate-buffered saline (PBS, pH 7.4) solution was prepared as the cleaning buffer solution and 0.01 M PBS (pH 7.4) containing 1%wt BSA was used as the blocking buffer. All other reagents were of analytical grade. All the aqueous solutions were prepared using ultra-pure water (Milli-Q, Millipore). The serum samples of individuals were kindly donated by the Affiliated Hospital of Qingdao University which have been approved by the Ethics Committee of the Affiliated Hospital of Qingdao University (QYFY WZLL 27,102).

Apparatus

Images from transmission electron microscopy (TEM) and scanning electron microscopy (SEM) were recorded from H-800 microscope (Hitachi, Japan) and Zeiss Supra 55 scanning electron microscope, respectively. Cyclic voltammetry (CV) and electrochemical impedance spectroscopy (EIS) analysis were conducted by CHI660B electrochemical workstation (Shanghai CH Instruments Corporation, China). The electrolyte solution consist 5 mM $K_3Fe(CN)_6/K_4Fe(CN)_6$ and 1.0 M KCl. The frequency used in EIS ranged from 0.01 Hz to100 kHz. ECL responses were obtained with an MPI-E multifunctional electrochemical and chemiluminescent analytical system (Remax Electronic Instrument Limited Co., Xi'an, China) using − 600 V as the voltage of the photomultiplier tube (PMT). All the electrochemical tests employed a conventional three-electrode system containing a bare or modified FTO electrode as working electrode, an Ag/AgCl electrode as reference electrode, and a Pt wire as the counter electrode. Nanocomposite characterization was performed by a UV–vis spectrophotometer (Cary 60, Agilent) in the experiments.

Synthesis of hemin-modified GO

H-RGO was synthesized based on a previous published method [34]. Detailed material synthesis is shown in the Supporting Information.

Synthesis of H-RGO-Au nanoflowers

The H-RGO-AuF partly was prepared using our previously reported method [34] and detailed material synthesis is shown in the Supporting Information.

Preparation of H-RGO-AuF/GOD/Ab_2 nanocomposites

The H-RGO-AuF/GOD/Ab_2 nanocomposites were synthesized as follows. One hundred twenty-five microliters of different concentration ratio of GOD and Ab_2 were mixed with 1 mL H-RGO-AuFs at 4 °C with continuous gently stirring for 4 h. Then, the products were collected by centrifugation at 12,000 rpm for 20 min and redispersed in 1 mL 0.01 mol L^{-1} PBS (pH 7.4). During the process, UV–vis absorption spectra was employed for every step characterization of the building-up process of Ab_2-probe.

Preparation of Au nanoflower–modified FTO electrode

The AuF-modified FTO electrodes were prepared according to a published method [36]. Detailed material synthesis is shown in the Supporting Information.

Preparation of ECL biosensor

The Au nanoflower–modified FTO FTO-AuF electrodes were firstly kept in PBS solution containing 5 mM thioglycolic acid for 6 h at 4 °C to introduce more carboxyl groups on their surface. After rinsing and drying with nitrogen, the electrodes were immersed into imidazole–HCl buffer solution which contains 30 mg mL^{-1} EDC and 15 mg mL^{-1} NHS and kept for 1 h to make the carboxyl groups activated. Then, to immobilize the Ab_1, 20 µL Ab_1 was dropped onto the electrode and kept static overnight at 4 °C. After washing off the nonspecific adsorb, the electrode was then incubated with 1% BSA for 1 h to prevent the nonspecific adsorption. The modified electrodes were then treated with various concentrations of PSA solutions at 37 °C for 1.5 h to capture the antigen. After this, H-RGO-AuFs/GOD/Ab_2 probe (Ab_2-probe) was introduced onto electrodes surface by the incubation with H-RGO-AuFs/GOD/Ab_2 solution at 37 °C for 1 h through the formation of sandwich structure (FTO-AuFs/Ab_1/BSA/PSA/Ab_2-probe). EIS and CV were performed to characterize each step of the modification process.

Specificity text and practicability in real serum sample analysis

The specificity text was constructed using solutions containing 2.5 ng mL^{-1} PSA and interfering proteins (250 ng mL^{-1} AFP and CEA, 50 mg mL^{-1} BSA) separately or mixed solution. The accuracy of developed biosensor was confirmed by measuring the concentration of PSA in real serum samples provided by the Affiliated Hospital of Qingdao University. The concentrations of PSA in these serum samples were previously tested by detected by ROCHE ELISA ECL analyzer at the Hospital which were regarded as the standard value. The original concentration of PSA ranged from 0.26 to 7.1 ng mL^{-1}. After receiving the patient's blood sample from the Affiliated Hospital of Qingdao University, the sample was put into a vacuum blood collection tube for coagulation, and then centrifuged at 4000 rpm for 5 min

at 4 ℃. The upper light yellow layer (approximately 1 mL) was transferred into a centrifuge tube and stored at 4 ℃. The ECL responses of the serum samples were measured after incubation of modified electrodes at 37 °C for 1.5 h. ECL responses were obtained with an MPI-E multifunctional electrochemical and chemiluminescent analytical system using – 600 V as the voltage of the PMT. The ECL detection electrolyte is 0.1 M pH 7.4 PBS containing 0.1 mM luminol and 0.01 M glucose; potential, – 1.3 V (vs Ag/AgCl); scan rate, 100 mV s^{-1}. Finally, the results of ECL signals were compared with the standard value obtained from ROCHE ELISA ECL analyzer. The recovery experiment was studied by adding fixed concentrations of PSA (0.25, 2.5, and 25 ng mL^{-1}) in three serum samples. These samples were appropriately prediluted with 0.1 M phosphate-buffered solution (pH 7.4) before the test. The original concentrations of un-spiked serum samples were obtained previously (ELISA ECL analyzer at hospital). The ECL results were detected by this method and were compared with standard value to calculate the recovery rate.

Results and discussion

Characterization of GO, H-RGO-AuNF nanocomposites, and FTO-AuF electrode

TEM images were first applied to demonstrate the morphology of GO and the synthesized ternary composites. Figure 1A shows a thin and wrinkled layer structure of GO. With further modification of hemin by heating and decoration with AuFs, the synthesized composites H-RGO-AuFs retain its layered structure as shown in Fig. 1B. The AuFs were uniformly dispersed on the GO surface without aggregation, and the diameter of AuFs was in the range of 75–100 nm. Moreover, FTO glasses after attachment of AuFs in situ through an electrochemical reduction technique were selected as the working electrodes. Figure 1C shows that the synthesized AuFs densely covered the FTO glass and kept a uniform shape. The above results indicate that we have successfully synthesized ternary composites H-RGO-AuFs and AuF-modified FTO glass.

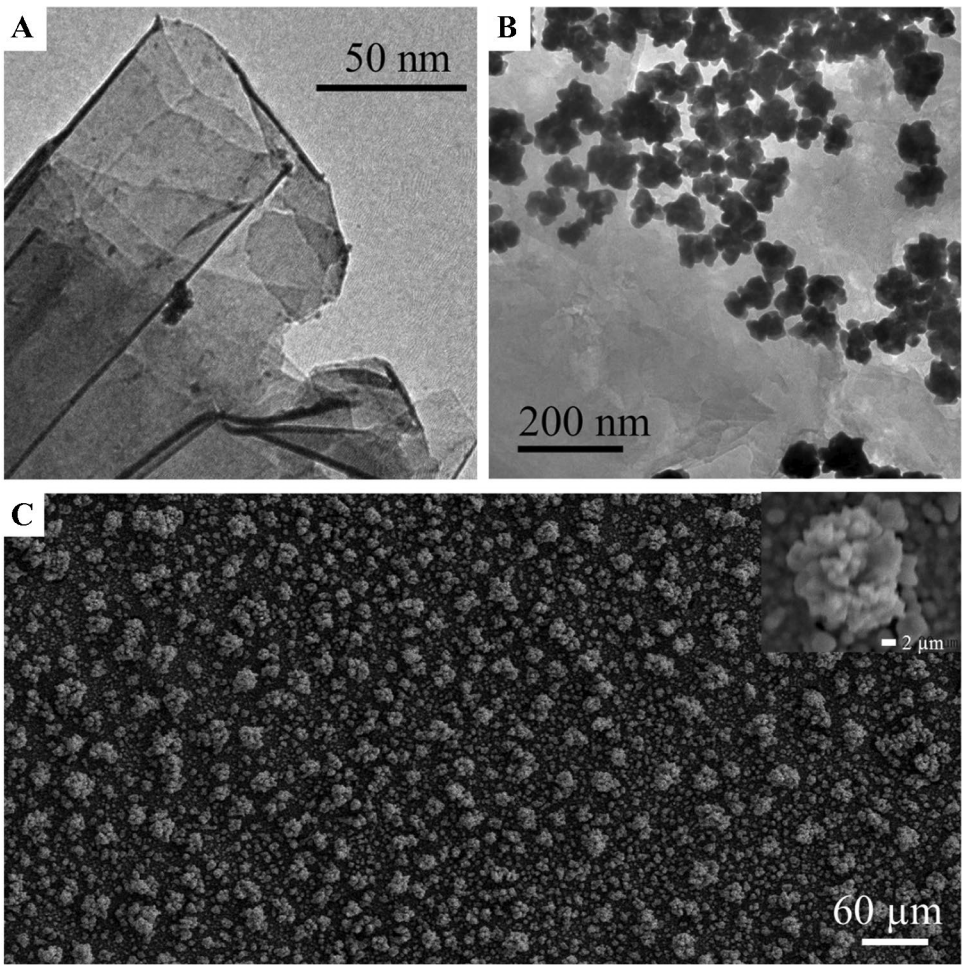

Fig. 1 TEM images of graphene oxide (**A**) and the synthesized ternary composites H-RGO-AuFs (**B**); **C** SEM images of the AuFs modified FTO glass. The inset image is a high-magnification image of AuFs

UV–vis absorption spectra were then used to monitor the nanocomposite synthesis. As shown in Fig. S1, after modification with hemin and AuFs, H-RGO-AuFs showed three typical peaks at 275 nm, 425 nm, and 602 nm which are consistent with our previous results [35] and demonstrated the successful modification of hemin and AuFs on the GO surface. After further attachment of Ab_2 and GOD, the H-RGO-AuFs/GOD/Ab_2 presented all their features as circled in its magenta curve in Fig. S1, indicating the successful synthesis of final probes.

Electrochemical measurements of stepwise modified ECL sensor

EIS and CVs were employed to monitor the assembly process of proposed FTO-based ECL sensor with $[Fe(CN)_6]^{3-/4-}$ as the active probes. Figure 2A displayed the electron transfer resistance, R_{et}, which derived from the semicircle domains of impedance spectra, increased gradually after step-by-step modification. The AuFs decorated FTO glass displayed an almost straight line owing to its good conductivity (curve a). After Ab_1, BSA, and PSA were assembled on the FTO-AuF surface, the R_{et} increased from 1932 Ω (data obtained from curve b) to 2261 Ω (data obtained from curve c) and 3250 Ω (data obtained from curve d), respectively. The increased EIS response could be attributed to the poor conductivity of such Ab_1, BSA, and PSA biomolecules. After capturing the Ab_2-probe through the specific identification between Ab_2 and PSA, an obviously increased R_{et} was observed (curve e) indicating that the synthesized Ab_2-probe blocked the electron transfer on the sensing interface due to the poor conductivity of such Ab_1, BSA, PSA, Ab_2, and GOD biomolecules. This suggested that the synthesized Ab_2-probe conjugates could be successfully bound to the sensing surface through the formation of sandwich structure between the PSA target and Ab.

The electrochemical kinetics of this ECL sensor during the fabrication process was valued through CV. From Fig. 2B, we could see that the CV of FTO-AuFs exhibited obvious redox peaks (curve a); these redox signals were subsequently depressed after the immobilization of Ab_1 (curve b), BSA (curve c), PSA biomolecules (curve d), and Ab_2-probe (curve e), which were consistent with the EIS measurements. The suppression of the redox peaks was probably due to the blocking effect from the attached biomolecules to the access of electrolyte ions required to balance the change in charge distribution which evidenced the successful stepwise modification of this ECL sensor.

Electrocatalytic activity of the fabricated ECL biosensor

To invesitigate the feasibility of the fabricated ECL biosensor, the ECL signal-time curves at different steps were recorded during the construction process. As shown in Fig. 3A, no ECL signal was observed from the FTO-AuF substate (curve a), and after modification with Ab_1, BSA, and PSA, a slight signal response was found (curve b–d). However, after further modification of Ab_2-probes on the working electrode via the speficic recognization between PSA and Ab_2, the ECL intensity significantly enhanced as shown with curve e. This phenomenon indicated that the attached Ab_2-probe catalyzed the glucose in solution to onsite generate coreactant H_2O_2 for the luminol-H_2O_2 system.

In order to enhance the biocatalytical efficiency of the fabricated biosensor, the optimal parameters in the experiments such as concentration ratio of GOD/Ab_2 and glucose concentration were studied and selected 40:1 and 0.01 M as the optimized concentration ratio of GOD/Ab_2, and concentration of glucose, respectively (Fig. S2). The stability of this PSA ECL sensor was also investigated by consecutive cyclic potential scans for 10 cycles in the presence of 0.5 ng mL^{-1} PSA. Figure 3B showed the observed stable ECL signals during the measurement.

ECL measurement of PSA activity

The performance of this ECL aptasensor for PSA detection was studied under the optimized experimental conditions in 0.1 M PBS (pH 7.4) with 0.1 mM luminol and 0.01 M

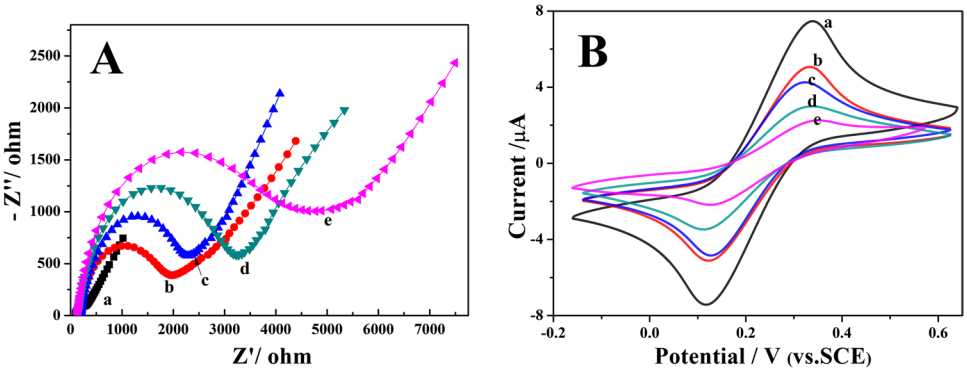

Fig. 2 **A** EIS and (**B**) CVs of the stepwise modified ECL sensor at different stages: (**a**) FTO-AuFs, (b) FTO-AuFs/Ab_1, (**c**) FTO-AuFs/Ab_1/BSA, (**d**) FTO-AuFs/Ab_1/BSA/PSA, and (**e**) FTO-AuFs/Ab_1/BSA/PSA/Ab_2-probe. All measurements were performed in 5 mM $[Fe(CN)_6]^{3-/4-}$ and 0.1 M KCl solution at room temperature

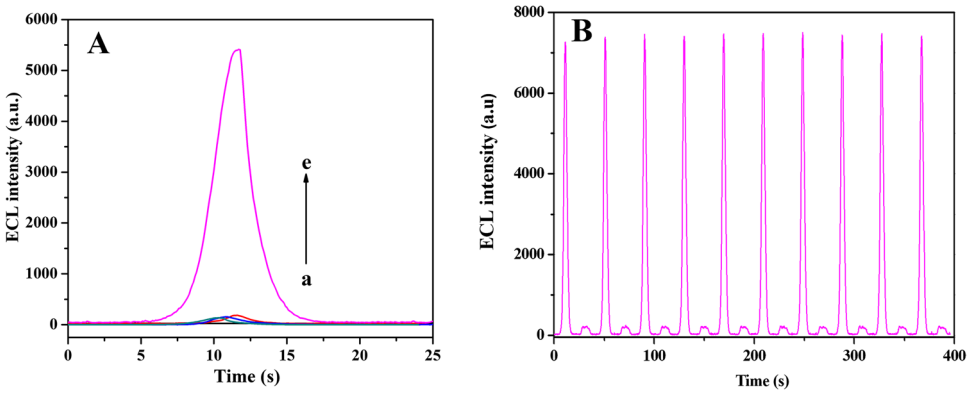

Fig. 3 **A** ECL characterization of the step-wise modified ECL sensor at different stages: (**a**) FTO-AuFs, (**b**) FTO-AuFs/Ab_1, (**c**) FTO-AuFs/Ab_1/BSA, (**d**) FTO-AuFs/Ab_1/BSA/PSA, and (**e**) FTO-AuFs/Ab_1/BSA/PSA/Ab_2-probe. (**B**) ECL emission of FTO-AuFs/Ab_1/BSA/PSA/Ab_2-probe under continuous cyclic potential scan for 10 cycles with 0.5 ng PSA. The detection solution: 0.1 M PBS (pH 7.4) containing 0.1 mM luminol and 0.01 M glucose. The PMT voltage: – 600 V. Potential: – 1.3 V (vs Ag/AgCl). Scan rate, 100 mV s^{-1}

glucose. Curve a of Fig. 4A showed that no obvious ECL signal was found in the electrolyte without PSA molecules. Apparently, the synthesized Ab_2-probe could not be bound to the working electrodes without the recognition between Ab_1, PSA, and Ab_2 molecules. With the increased PSA concentration, as expected, the ECL signals increased accordingly in the range of 7.5×10^{-4} to 2.5 ng mL^{-1} of PSA (from curve b to h in Fig. 4A). Figure 4B demonstrates the liner relationship between ECL readout (I) and the logarithm of PSA concentration (C_{PSA}) in the range of 7.5×10^{-4} to 2.5 ng mL^{-1} of PSA. The linear equation is $I = 8390.78 + 2690.87 \log C_{PSA}$ (ng mL^{-1}) with a correlation coefficient of 0.995. The limit of detection was calculated to be 0.32 pg mL^{-1} with a signal to noise ratio of 3. In comparison to previously reported immunosensing work using gold nanoparticles, MOF, or $CdTe/TiO_2$ nanomaterials, this work showed comparable or lower detection limit. The linear detection range of the proposed method with 4 orders of magnitude is also wider enough to meet the requirement of clinic detection. The detailed comparison and discussion of the superiority of this work with previous sensing method including electrochemical, ECL, photoelectrochemical, fluorescent, and SPR are listed in Table S1. The enhanced performance may be attributed to the excellent performance of the GO@AuNRs-GOD-SA-Biotin-DNA in the luminol-based ECL system.

We further studied whether other interfering biomolecules affect the sensing analysis for the target in this ECL biosensor. The specific measurement was carried out using BSA, CEA, AFP, and mixed samples (PSA:BSA:CEA:AFP = $1:2\times10^7$:100:100) in the detection system. As illustrated in Fig. 5, no obvious ECL signal was observed on FTO-AuF/Ab_1/BSA substrate and AFP- and CEA-treated substrates, whereas the ECL response of the mixture containing the above interfering proteins and PSA has no obvious differences with that of the target only, suggesting the good specificity of the immunosensing platform. Benefiting from the specific identification between Ab_1, PSA, and Ab_2, the presented sensor is expected to sensitive to PSA only.

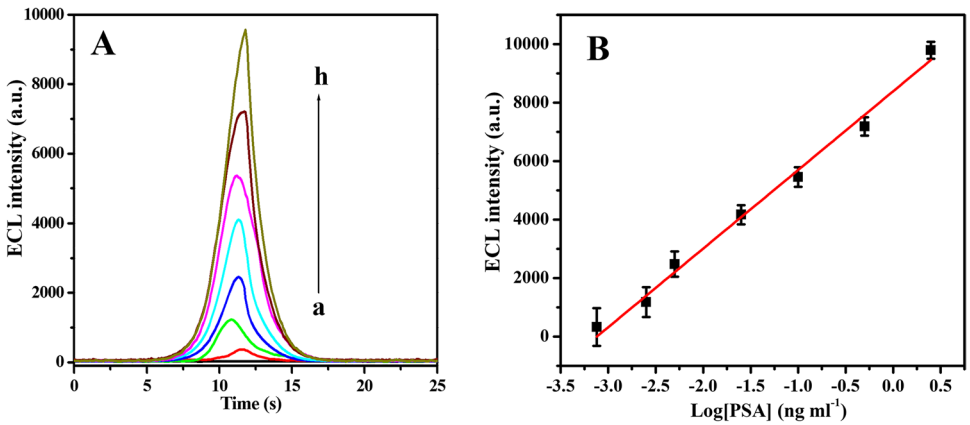

Fig. 4 **A** ECL signals intensity of this strategy for detection of different concentrations of the PSA (0, 7.5×10^{-4}, 2.5×10^{-3}, 5×10^{-3}, 25×10^{-3}, 0.1, 0.5, 2.5 ng mL^{-1} from curve a to curve h respectively). (**B**) The relationship between the ECL signals intensity and the logarithm of PSA concentration from 7.5×10^{-4} to 2.5 ng mL^{-1}. The detection electrolyte: 0.1 M PBS (pH 7.4) containing 0.1 mM luminol and 0.01 M glucose. Scan rate, 100 mV s^{-1}

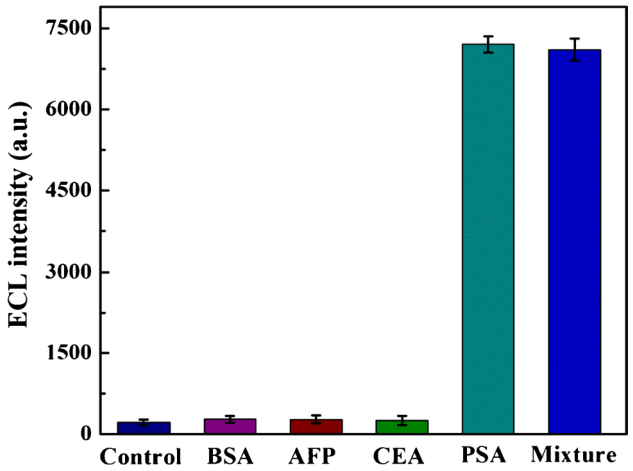

Fig. 5 Specificity of the proposed strategy for PSA detection. Error bars were estimated from three independent replicate measurements. (PSA: 2.5 ng mL^{-1}, BSA: 50 mg mL^{-1}, AFP: 250 ng mL^{-1}, CEA: 250 ng mL^{-1}, the detection electrolyte: 0.1 M pH 7.4 PBS containing 0.1 mM luminol and 0.01 M glucose)

Table 1 Recovery of PSA in human serum samples

Sample no	Found (ng/mL)	Added (ng/mL)	Total found (ng/mL)	Recoveries (%)	RSDs (%, $n=3$)
1	0.26	0.25	0.57	111.8	4.7
2	0.37	2.5	2.6	90.6	3.9
3	1.8	25	27	100.7	5.5

Analysis of real sample analysis

In order to evaluate the feasibility of the constructed immunosensing method, seven human serum samples were determined. The concentrations of PSA in these seven serum samples were previously tested by detected by ROCHE ELISA ECL analyzer at the Hospital which were regarded as the standard value. The experiment was done in parallel with at least three groups. Table S2 shows the data obtained by the proposed method and the provided standard values. The relative errors between the two methods are less than 10.2% and RSDs are below 9.7%. Furthermore, the recovery of the method was also examined by spiking PSA with different concentrations (0.25, 2.5, and 25 ng mL^{-1}) into three serum samples, respectively. As listed in Table 1, the recoveries range from 90.6 to 111.8%, and the RSDs are no more than 5.5%, validating the reliability and practicality of this method as a promising potential application prospect for the detection of PSA in clinical diagnosis.

Conclusion

In conclusion, an ultrasensitive graphene oxide–based ECL biosensor was built for PSA detection. The H-RGO-AuF ternary nanocomposites were first synthesized and then found excellent catalytic enhancement towards peroxidase mimetics due to the superior conductivity of graphene and nanosucculents of AuFs. It is evident that this ECL immunosensor with ternary nanocomposites as probes performs sensitive and accurate detection of PSA, and we believe that these decorated H-RGO-AuF ternary nanocomposites can serve as versatile platforms for studies and application in biomedical diagnosis. However, there are still challenges in the application of clinic detection which provide future topic, for example, how to simplify the electrode preparation process and find strategies for more portable electrode to realize point-of-care testing. Additionally, high-throughput simultaneous detection for multiple biomarkers in one sample based on spatial, potential, or spectrum-resolved ECL technologies is another hot topic with the increasing need for accurate cancer diagnosis and prediction in clinic detection.

Supplementary Information The online version contains supplementary material available at https://doi.org/10.1007/s00604-022-05387-2.

Acknowledgements We thank all the patients and colleagues who contributed to the study.

Funding This work was supported by the National Natural Science Foundation of China (Grant No. 21675074) and the Shandong Natural Science Foundation of Shandong (ZR2017MH042), Shandong Traditional Chinese Medicine Science and Technology Development Plan Project (2017–202).

Declarations

Conflict of interest The authors declare no competing interests.

References

1. Wu L, Qu X (2015) Cancer biomarker detection: recent achievements and challenges. Chem Soc Rev 44:2963–2997. https://doi.org/10.1039/c4cs00370e
2. Huang X, Liu Y, Yung B et al (2017) Nanotechnology-enhanced no-wash biosensors for in vitro diagnostics of cancer. ACS Nano 11:5238–5292. https://doi.org/10.1021/acsnano.7b02618
3. Wu X, Hao C, Kumar J et al (2018) Environmentally responsive plasmonic nanoassemblies for biosensing. Chem Soc Rev 47:4677–4696. https://doi.org/10.1039/c7cs00894e
4. Husain RA, Barman SR, Chatterjee S et al (2020) Enhanced biosensing strategies using electrogenerated chemiluminescence: recent progress and future prospects. J Mater Chem B 8:3192–3212. https://doi.org/10.1039/c9tb02578b

5. Kal-Koshvandi AT (2020) Recent advances in optical biosensors for the detection of cancer biomarker alpha-fetoprotein (AFP). Trac-Trend Anal Chem 128:115920. https://doi.org/10.1016/j.trac.2020.115920
6. Ma F, Li Y, Tang B, Zhang CY (2016) Fluorescent biosensors based on single-molecule counting. Acc Chem Res 49:1722–1730. https://doi.org/10.1021/acs.accounts.6b00237
7. Zhou H, Liu J, Xu JJ et al (2018) Optical nano-biosensing interface via nucleic acid amplification strategy: construction and application. Chem Soc Rev 47:1996–2019. https://doi.org/10.1039/c7cs00573c
8. Tang L, Li J (2017) Plasmon-based colorimetric nanosensors for ultrasensitive molecular diagnostics. ACS Sens 2:857–875. https://doi.org/10.1021/acssensors.7b00282
9. Du FX, Chen YQ, Meng CD et al (2021) Recent advances in electrochemiluminescence immunoassay based on multiple-signal strategy. Curr Opin Electrochem 28:100725. https://doi.org/10.1016/j.coelec.2021.100725
10. Wang Y, Zhao GH, Chi H et al (2021) Self-luminescent lanthanide metal-organic frameworks as signal probes in electrochemiluminescence immunoassay. J Am Chem Soc 143:504–512. https://doi.org/10.1021/jacs.0c12449
11. Wang B, Shi S, Yang X et al (2020) Separation-free electrogenerated chemiluminescence immunoassay incorporating target assistant proximity hybridization and dynamically competitive hybridization of a DNA signal probe. Anal Chem 92:884–891. https://doi.org/10.1021/acs.analchem.9b03662
12. Hong D, Jo E-J, Kim K et al (2020) $Ru(bpy)_3^{2+}$-loaded mesoporous silica nanoparticles as electrochemiluminescent probes of a lateral flow immunosensor for highly sensitive and quantitative detection of troponin I. Small 16:2004535. https://doi.org/10.1002/smll.202004535
13. Khoshfetrat SM, Hashemi P, Afkhami A et al (2021) Cascade electrochemiluminescence-based integrated graphitic carbon nitride-encapsulated metal-organic framework nanozyme for prostate-specific antigen biosensing. Sens Actuators, B Chem 348:130658. https://doi.org/10.1016/j.snb.2021.130658
14. Jia HY, Yu SQ, Yang L et al (2021) Near-infrared electrochemiluminescence of dual-stabilizer-capped Au nanoclusters for immunoassays. Acs Appl Nano Mater 4:2657–2663. https://doi.org/10.1021/acsanm.0c03284
15. Yu L, Zhang Q, Kang Q et al (2020) Near-infrared electrochemiluminescence immunoassay with biocompatible Au nanoclusters as tags. Anal Chem 92:7581–7587. https://doi.org/10.1021/acs.analchem.0c00125
16. Hong GL, Su CP, Huang ZN et al (2021) Electrochemiluminescence immunoassay platform with immunoglobulin G-encapsulated gold nanoclusters as a "two-in-one" probe. Anal Chem 93:13022–13028. https://doi.org/10.1021/acs.analchem.1c02850
17. Kannan P, Chen J, Su FM et al (2019) Faraday-cage-type electrochemiluminescence immunoassay: a rise of advanced biosensing strategy. Anal Chem 91:14792–14802. https://doi.org/10.1021/acs.analchem.9b04503
18. Song Y, Zhang W, He SJ et al (2019) Perylene diimide and luminol as potential-resolved electrochemiluminescence nanoprobes for dual targets immunoassay at low potential. ACS Appl Mater Interfaces 11:33676–33683. https://doi.org/10.1021/acsami.9b11416
19. Cao J-T, Fu X-L, Zhao L-Z, et al (2020) Highly efficient resonance energy transfer in g-C_3N_4-Ag nanostructure: proof-of-concept toward sensitive split-type electrochemiluminescence immunoassay. Sens Actuators B-Chem 311:127926. https://doi.org/10.1016/j.snb.2020.127926
20. Wang WX, Liu YH, Shi TH et al (2020) Biosynthesized quantum dot for facile and ultrasensitive electrochemical and electrochemiluminescence immunoassay. Anal Chem 92:1598–1604. https://doi.org/10.1021/acs.analchem.9b04919
21. Liu Q, Liu XP, Wei YP et al (2017) Electrochemiluminescence immunoassay for the carcinoembryonic antigen using CdSe: Eu nanocrystals. Microchim Acta 184:1353–1360. https://doi.org/10.1007/s00604-017-2114-6
22. Qin DM, Jiang XH, Mo GC, et al (2020) Electrochemiluminescence immunoassay of human chorionic gonadotropin using silver carbon quantum dots and functionalized polymer nanospheres. Microchim Acta 187:482. https://doi.org/10.1007/s00604-020-04450-0
23. Wang XF, Gao HF, Qi HL et al (2018) Proximity hybridization-regulated immunoassay for cell surface protein and protein-overexpressing cancer cells via electrochemiluminescence. Anal Chem 90:3013–3018. https://doi.org/10.1021/acs.analchem.7b04359
24. Ge JJ, Zhao Y, Li CL, Jie GF (2019) Versatile electrochemiluminescence and electrochemical "on-off" assays of methyltransferases and aflatoxin B1 based on a novel multifunctional DNA nanotube. Anal Chem 91:3546–3554. https://doi.org/10.1021/acs.analchem.8b05362
25. Wang C, Li ZH, Ju HX (2021) Copper-doped terbium luminescent metal organic framework as an emitter and a co-reaction promoter for amplified electrochemiluminescence immunoassay. Anal Chem 93:14878–14884. https://doi.org/10.1021/acs.analchem.1c03988
26. Chen Y, Zhou SW, Li LL, Zhu JJ (2017) Nanomaterials-based sensitive electrochemiluminescence biosensing. Nano Today 12:98–115. https://doi.org/10.1016/j.nantod.2016.12.013
27. Yildiz G, Bolton-Warberg M, Awaja F (2021) Graphene and graphene oxide for bio-sensing: general properties and the effects of graphene ripples. Acta Biomater 131:62–79. https://doi.org/10.1016/j.actbio.2021.06.047
28. Song YJ, Qu KG, Zhao C et al (2010) Graphene oxide: intrinsic peroxidase catalytic activity and its application to glucose detection. Adv Mater 22:2206–2210. https://doi.org/10.1002/adma.200903783
29. Zhao Y, Zhang YQ and Jie GF (2021) An "on-off' electrochemiluminescence biosensor based on DNA nanotweezer probe coupled with tripod capture DNA for high sensitive detection of Pb^{2+}. Sens Actuators B-Chem 326:128985. https://doi.org/10.1016/j.snb.2020.128985
30. Pothipor C, Jakmunee J, Bamrungsap S, Ounnunkad K (2021) An electrochemical biosensor for simultaneous detection of breast cancer clinically related microRNAs based on a gold nanoparticles/graphene quantum dots/graphene oxide film. Analyst 146:4000–4009. https://doi.org/10.1039/d1an00436k
31. Cao JT, Yang JJ, Zhao LT et al (2018) Graphene oxide@gold nanorods-based multiple-assisted electrochemiluminescence signal amplification strategy for sensitive detection of prostate specific antigen. Biosens Bioelectron 99:92–98. https://doi.org/10.1016/j.bios.2017.07.050
32. Liu WY, Yang HM, Ge SG et al (2015) Application of bimetallic PtPd alloy decorated graphene in peroxydisulfate electrochemiluminescence aptasensor based on Ag dendrites decorated indium tin oxide device. Sens Actuators B-Chem 209:32–39. https://doi.org/10.1016/j.snb.2014.11.079
33. Dong YL, Zhang HG, Rahman ZU et al (2012) Graphene oxide-Fe3O4 magnetic nanocomposites with peroxidase-like activity for colorimetric detection of glucose. Nanoscale 4:3969–3976. https://doi.org/10.1039/c2nr12109c
34. Liu J, Cui MR, Niu L et al (2016) Enhanced peroxidase-like properties of graphene-hemin-composite decorated with Au nanoflowers as electrochemical aptamer biosensor for the detection of K562 leukemia cancer cells. Chem-a Euro J 22:18001–18008. https://doi.org/10.1002/chem.201604354

35. Liu J, Zhai FF, Zhou H, et al (2019) Nanogold flower-inspired nanoarchitectonics enables enhanced light-to-heat conversion ability for rapid and targeted chemo-photothermal therapy of a tumor. Adv Healthcare Mater 8. https://doi.org/10.1002/adhm.201801300
36. Zhou H, Ding KX, Yu Q, et al (2021) Enhanced electrochemiluminescence ratiometric cytosensing based on surface plasmon resonance of Au nanoparticles and nanosucculent films. Biosens Bioelectro 189. https://doi.org/10.1016/j.bios.2021.113367